Available online at www.sciencedirect.com
SCIENCE DIRECT
Journal of Molecular Structure 785 (2006) 192–204
Journal of MOLECULAR STRUCTURE
www.elsevier.com/locate/molstruc

Vibrational assignment and dipole moment derivatives of hexafluorobenzene between 4000 and 250 cm^{-1}

C.Dale Keefe *, Shaun Mac Innis

Department of Physical and Applied Sciences, Cape Breton University Sydney, NS, Canada B1P 6L2

Received 16 August 2005; received in revised form 10 October 2005; accepted 11 October 2005
Available online 17 November 2005

Abstract

The liquid phase vibrational assignment and dipole moment derivatives of hexafluorobenzene are reported. These are obtained by fitting the imaginary molar polarizability spectrum of hexafluorobenzene to classical damped harmonic oscillator bands. Most of the observed transitions were assigned to infrared active fundamentals or binary combinations. From the active combination transitions, the wavenumbers of the inactive fundamentals were obtained. In addition, ab initio calculations at the CCD/cc-pVDZ level of theory were used to determine the harmonic force field and dipole moment derivatives of gaseous hexafluorobenzene. It was determined that in the gas phase $\partial\mu_y/\partial s_1 = -5.53$ Debye $Å^{-1}$, $\partial\mu_x/\partial t_2 = 1.03$, $\partial\mu_x/\partial\beta_1 = 0.78$, and $\partial\mu_z/\partial\gamma_1 = 0.57$ Debye $Å^{-1}$ while in the liquid $\partial\mu_y/\partial s_1 = -4.00$ Debye $Å^{-1}$, $\partial\mu_x/\partial t_2 = 1.27$, and $\partial\mu_x/\partial b_1 = 0.50$ Debye $Å^{-1}$. $\partial\mu_z/\partial\gamma_1$ could not be determined for the liquid phase because the fundamental is below the limits of the current measurements. The differences between the liquid and gas phase dipole moment derivatives of hexafluorobenzene were found to be consistent with the differences previously reported for benzene.

1. Introduction

Over the last 10 years, this laboratory has been involved in the exploration of the absolute infrared vibrational intensities of benzene and benzene derivatives in the liquid phase. The focus of this project is to better understand how the intermolecular interactions in the liquid affect the vibrational intensities. Interest in the vibrational properties of benzene dates back to the 1930s with the work of Wilson [1].

The integrated intensities in the liquid phase are obtained from the imaginary molar polarizability spectrum, which is determined from the complex refractive index spectra across the infrared. For a review of how one obtains complex refractive index spectra and the conversion to the imaginary molar polarizability spectrum, the reader is referred to Ref. [2] and references cited therein. Once the imaginary molar polarizability spectrum is known, the integrated intensities of the various transitions need to be determined. This is done by fitting the imaginary molar polarizability spectrum to a standard lineshape. The preferred [2–4] lineshape for the imaginary molar polarizability spectrum is the classical damped harmonic oscillator (CDHO) lineshape. From the integrated intensities, the transition moments and dipole moment derivatives can be obtained. It is these quantities that are compared between the different benzene compounds to gain insight into how the liquid phase vibrational intensities are dependent upon the intermolecular interactions.

To date, the complex refractive index spectra, imaginary molar polarizability spectra, transition moments and dipole moment derivatives have been reported for benzene [5–7], benzene-d_6[8], benzene-d_1[9], bromobenzene [10,11], bromobenzene-d_5 [12,13], and toluene [14,15]. In addition, the complex refractive index spectra and imaginary molar polarizability spectra of hexafluorobenzene [16], ethylbenzene [17], fluorobenzene [18], and toluene-d_8 [19] have been reported. Work is presently underway to fit the imaginary molar polarizability spectra of these compounds.

Additionally, the experimental intensities and force field of three isotopomers of liquid benzene (-h_6, -d_6, -d_1) have been used to determine the dipole moment derivatives with respect to symmetry and internal coordinates [20]. These dipole moment derivatives were compared to the corresponding experimental derivatives of gaseous benzene [21]. It was found that while the experimental intensities are different for the three isotopomers in the liquid and gas phase, these differences are due essentially to a difference in the CH stretch dipole moment derivative. This difference was related qualitatively to the intermolecular interaction of the H with

* Corresponding author. Tel.: +1 902 563 1185; fax: +1 902 563 1880.
E-mail address: dale_keefe@capebretonu.ca (C.D. Keefe).

0022-2860/$ - see front matter © 2006 Elsevier B.V. All rights reserved.
doi:10.1016/j.molstruc.2005.10.010

Table 1
Observed and fitted bands in the imaginary molar polarizability spectrum of liquid hexafluorobenzene

Assignment[a]		Obsd $\tilde{\nu}$[b]	Fitted band			Sum of C_j[c]
Present works	Ref. [36]		$\tilde{\nu}$[d]	Γ_j[d]	C_j[c]	
		3963 VW	3963.5	24.2	158.1	
		3903 VW	3902.9	32.5	31.7	
		3864 VW Sh	3864.8	28.0	26.7	
		3839 VW Sh	3839.1	23.3	51.6	
		3826 VW	3825.3	22.0	107.1	
		3805 VW Sh	3803.4	22.2	61.4	
		3736 VW Sh	3735.2	19.6	14.4	
		3723 VW	3722.3	15.5	22.4	
		3700 VW	3700.8	13.3	2.7	
		3661 VW Sh	3664.1	22.2	21.3	
		3631 VW	3630.9	19.7	185.8	
		3580 VW Sh	3578.1	8.9	8.4	
		3571 VW	3571.0	10.0	17.6	
			3561.2	13.7	13.4	
		3539 VW	3540.8	15.1	45.9	
		3527 VW Sh	3529.4	15.5	20.5	
		3512 VW Sh	3512.8	18.4	17.8	
			3506.6	28.2	2.3	
		3455 VW	3456.4	18.6	45.8	
		3419 VW	3419.8	18.3	21.0	
		3391 VW	3390.5	8.1	0.6	
		3374 VW Sh	3372.1	14.1	8.5	
		3364 VW	3362.2	9.6	6.1	
		3325 VW Sh	3328.1	19.5	38.0	
		3307 VW Sh	3311.8	15.8	35.4	
		3298 VW	3301.3	12.7	36.9	
		3295 VW Sh	3292.8	14.0	39.1	
		3242 VW	3245.2	12.4	58.5	
			3237.4	12.8	42.2	
		3187 VW Sh	3184.9	12.6	20.5	
$\nu_{12}+\nu_{15}$ (3186,5E_{1u})	$\nu_{12}+\nu_{15}$	3177 VW	3177.7	11.9	361.6	
			3172.1	10.8	103.5	
		3157 VW Sh	3156.5	7.9	3.5	
			3132.9	11.8	35.7	
		3126 VW	3125.9	10.5	40.7	
		3119 VW Sh	3118.6	10.3	30.5	
		3108 VW Sh	3109.4	10.3	20.2	
			3101.2	9.1	17.0	
			3094.3	7.5	17.7	
			3089.5	6.1	19.8	
		3084 VW	3085.6	5.8	22.6	
		3082 VW Sh	3082.1	5.0	15.5	
		3078 VW Sh	3078.5	4.9	13.1	
		3075 VW Sh	3075.2	4.7	10.3	
		3072 VW Sh	3071.9	5.0	10.2	
		3067 VW Sh	3067.4	5.9	14.2	
		3062 VW Sh	3062.2	6.6	13.2	
		3056 VW Sh	3057.1	7.4	20.1	
		3054 VW	3052.8	12.0	50.0	
		3051 VW Sh	I			
		3031 VW Sh	3031.4	13.1	218.1	
$\nu_1+\nu_{12}$ (3021, E_{1u})	$\nu_1+\nu_{12}$	3025 W Sh	3025.6	8.5	263.2	
			3021.3	6.6	331.2	
		3016 W	3018.0	5.8	418.9	
		3013 W Sh	3014.9	5.9	461.7	
			3011.6	6.2	349.0	
		3004 VW Sh	3007.5	6.4	142.2	
			2987.5	3.1	139.5	
			2985.6	3.1	251.1	
		2984 W	2983.6	3.6	302.3	
		2981 W Sh	2981.2	4.8	333.0	

(*continued on next page*)

Table 1 (*continued*)

Assignment[a]		Obsd $\tilde{\nu}^b$	Fitted band			Sum of C_j^c
Present works	Ref. [36]		$\tilde{\nu}^d$	Γ_j^d	C_j^c	
$\nu_5+\nu_{15}$ (2977, E_{1u})	$\nu_5+\nu_{15}$	2977 W Sh	2977.9	8.1	301.7	
		2963 VW	2962.3	18.3	368.0	
		2941 VW Sh	2941.6	17.6	190.2	
		2930 VW	2929.9	14.0	195.3	
		2924 VW	2922.9	12.2	183.7	
		2914 VW Sh	2915.4	11.5	67.4	
$\nu_9+\nu_{15}$ (2097, E_{1u})	$\nu_9+\nu_{15}$	2906 W	2906.1	14.6	545.3	
		2889 VW Sh	2890.3	15.5	87.5	
		2880 VW Sh	2881.4	14.9	50.7	
		2855 VW Sh	2854.8	19.9	250.5	
		2845 VW Sh	I			
		2833 VW Sh	I			
		2809 VW	I			
		2797 VW	I			
		2751 VW	2752.4	5.4	2.7	
		2697 W Sh	2696.5	8.3	426.7	
		2692 W Sh	2691.0	7.4	840.2	
			2686.6	7.1	1391.2	
$\nu_{12}+\nu_{16}$ (2688, E_{1u})	$\nu_{12}+\nu_{16}$	2683 M	2682.7	7.5	1890.7	
			2678.6	9.3	1919.2	
		2671 W Sh	2671.5	14.1	835.2	
$\nu_{13}+\nu_{15}$ (2650, E_{1u})		2653 W Sh	2649.9	17.5	498.4	
		2614 VW Sh	2616.6	11.0	27.6	
		2610 VW	2608.6	10.0	39.2	
		2596 VW Sh	2598.6	9.0	32.6	
		2590 VW	2592.5	7.8	42.7	
			2586.9	8.1	41.7	
		2579 VW Sh	2579.8	9.9	27.7	
		2551 VW Sh	2551.6	13.7	72.7	
			2535.1	10.6	66.0	
		2531 VW Sh	2530.7	9.0	51.2	
			2516.7	8.0	130.8	
			2511.7	10.0	660.1	
$\nu_1+\nu_{13}$ (2485, E_{1u})	$\nu_1+\nu_{13}$	2508 W Sh	2506.3	10.1	535.7	
			2500.3	11.2	519.6	
			2492.2	9.5	489.8	
			2487.6	7.3	699.9	
$\nu_1+\nu_{13}$ (2485, E_{1u})			2484.2	6.1	1043.1	
			2481.5	5.7	1538.7	
$\nu_5+\nu_{16}$ (2477, E_{1u})	$\nu_1+\nu_{13,}$ $\nu_5+\nu_{16}$	2479 M	2478.9	6.1	1927.7	
			2476.0	7.1	1743.6	
		2470 W Sh	2471.9	8.1	678.9	
		2467 W Sh	2465.8	8.6	425.8	
		2424 W Sh	2425.3	17.1	587.6	
$\nu_9+\nu_{16}$ (2409, E_{1u})	$\nu_9+\nu_{16}$	2410 W Sh	2410.3	11.6	358.2	
		2405 W	2404.1	9.0	364.6	
			2398.1	9.1	215.9	
		2312 VW	2312.7	6.6	10.2	
$\nu_6+\nu_{15}$ (2296, E_{1u})		2296 VW	2297.9	4.7	4.4	
			2264.9	4.3	50.0	
			2262.4	3.3	94.8	
$\nu_{15}+\nu_{19}$ (2254, A_{2u})	$\nu_{15}+\nu_{19}$	2260 W	2260.6	3.0	155.1	
			2259.1	2.8	120.4	
			2257.5	3.2	101.8	
			2255.3	3.7	69.8	
			2253.4	5.9	0.2	
		2252 VW Sh	2252.3	4.8	49.1	
		2246 VW Sh	2246.0	6.7	40.9	
		2201 VW Sh	I			
	$\nu_{13}+\nu_{16}$	2177 W Sh	2177.3	12.9	558.1	
		2168 W Sh	2167.4	15.1	662.7	
			2153.0	13.4	846.6	
			2147.6	19.2	18.0	
$\nu_{13}+\nu_{16}$ (2152, E_{1u})	$\nu_{13}+\nu_{16}$	2149 W	2146.8	12.0	1026.1	

Assignment[a]		Obsd $\tilde{\nu}$[b]	Fitted band			Sum of C_j[c]
Present works	Ref. [36]		$\tilde{\nu}$[d]	Γ_j[d]	C_j[c]	
			2101.7	6.0	89.5	
			2097.6	5.0	147.2	
		2095 W Sh	2094.2	4.8	200.7	
			2091.1	4.7	271.4	
			2088.2	4.6	368.9	
$\nu_2+\nu_{12}$ (2090, E_{1u})	$\nu_2+\nu_{12}$	2084 W	2085.5	4.7	481.5	
			2082.7	5.2	566.6	
			2079.6	6.2	515.1	
			2075.0	8.2	246.8	
$\nu_5+\nu_7$ (2034, A_{2u})	$\nu_5+\nu_7$	2044 W	2044.1	3.0	24.7	
		2033 VW Sh	I			
		2019 VW	I			
		1992 VW Sh	I			
$\nu_{12}+\nu_{17}$ (1974, E_{1u})	$\nu_{12}+\nu_{17}$, $\nu_{14}+\nu_{15}$	1975 VW Sh	1976.1	5.9	68.6	
$\nu_{14}+\nu_{15}$ (1970, E_{1u})			1970.2	4.7	61.5	
		1968 VW	1966.6	4.3	57.8	
		1934 VW	1934.6	1.7	4.9	
		1914 VW Sh	I			
$\nu_{11}+\nu_{12}$ (1901, A_{2u})	$\nu_{11}+\nu_{12}$	1895 W	1895.3	10.3	271.1	
$\nu_{10}+\nu_{15}$ (1863, E_{1u})		1875 VW Sh	I			
$\nu_{15}+\nu_{20}$ (1831, E_{1u})	$\nu_{15}+\nu_{20}$	1839 VW	I			
$\nu_1+\nu_{14}$ (1805, E_{1u})	$\nu_{12}+\nu_{18}$, $\nu_6+\nu_{16}$, $\nu_1+\nu_{14}$	1805 W	1805.7	6.9	1510.5	
$\nu_{12}+\nu_{18}$ (1795, E_{1u}), $\nu_6+\nu_{16}$ (1798, E_{1u})		1795 W Sh	1800.6	9.8	921.9	
		1770 W Sh	1771.7	4.3	166.5	
			1768.7	3.9	234.7	
			1766.0	3.5	355.8	
			1764.1	3.1	395.5	
			1762.1	3.6	731.6	
$\nu_5+\nu_{17}$ (1765, E_{1u})		1759 M	1760.0	4.0	1121.6	
			1758.0	3.3	727.4	
			1756.3	2.9	449.9	
			1754.4	4.0	636.4	
$\nu_{16}+\nu\nu_{19}$ (1756, A_{2u})		1749 W Sh	1751.6	4.7	350.6	
		1746 W Sh	1747.8	6.1	190.5	
		1740 W Sh	1739.4	8.8	105.2	
			1720.8	6.6	232.5	
		1718 W Sh	1716.6	7.0	272.0	
	$\nu_3+\nu_{13}$	1708 W	1710.1	6.7	464.8	
$\nu_1+\nu_4$ (1705, A_{2u})			1705.6	7.6	444.4	
		1700 W Sh	I			
$\nu_9+\nu_{17}$ (1695, E_{1u})		1696 W Sh	I			
$\nu_3+\nu_{13}$ (1689, E_{1u})	$\nu_3+\nu_{13}$, $\nu_9+\nu_{17}$	1690 W	1690.7	8.3	776.5	
ν_{15} (1655, E_{1g})		1656 W Sh	I			
		1652 W	I			
		1643 W Sh	I			
$\nu_5+\nu_{18}$ (1586, E_{1u})	$\nu_5+\nu_{18}$	1596 M	1596.5	3.3	1149.2	
$\nu_5+\nu_8$ (1567, A_{2u})	$\nu_5+\nu_8$	1557 S Sh	1556.8	4.0	5111.5	
			1553.0	3.3	782.2	
$\nu_2+\nu_{13}$ (1554, E_{1u})	$\nu_2+\nu_{13}$	1551 S Sh	1551.5	2.2	1534.4	
		1546 S Sh	1547.3	8.7	14224.0	
		1540 S Sh	1539.5	7.1	63457.7	
		1538 S Sh	1538.5	0.2	1371.5	
		1536 VS Sh	1536.5	3.6	51843.8	
		1535 VS Sh	1535.0	1.7	19193.6	
		1534 VS Sh	1534.1	1.2	6768.5	
		1533 VS Sh	1533.6	1.8	15140.9	595220.6
		1532 VS Sh	1532.2	2.9	94533.2	
ν_{12} (E_{1u})	ν_{12}	1531 VS	1530.7	2.4	57075.0	
		1530 VS Sh	1529.8	0.5	3000.8	
		1529 VS Sh	1528.9	2.6	54679.4	
		1527 VS Sh	1527.3	4.0	116509.1	
		1524 VS Sh	1524.5	5.4	86434.8	
		1520 S Sh	1521.0	5.6	17756.8	
$\nu_9+\nu_{18}$ (1516, E_{1u})		1515 S Sh	1516.5	9.0	24633.2	

Table 1 (*continued*)

Assignment[a]		Obsd $\tilde{\nu}$[b]	Fitted band			Sum of C_j[c]
Present works	Ref. [36]		$\tilde{\nu}$[d]	Γ_j[d]	C_j[c]	

(*continued on next page*)

		1513 S Sh	I			
	$\nu_9+\nu_{18}$	1511 S Sh	I			
		1509 S Sh	I			
		1506 S Sh	1506.6	4.0	4260.6	
		1502 M Sh	1501.8	0.0	970.9	
ν_1 (1490, A_{1g})		1492 M Sh	1492.3	2.3	437.6	
	$\nu_{14}+\nu_{16}$	1489 M Sh	I			
$\nu_{15}-\nu_{20}$ (1479, A_{2u})		1482 M	1481.6	2.5	230.7	
$\nu_{14}+\nu_{16}$ (1472, E_{1u})	$\nu_{13}+\nu_{17}$	1466 M	1466.3	9.3	1770.5	
		1459 M Sh	1457.4	12.6	1828.0	
$\nu_{15}-\nu_{10}$ (1449, E_{1u})		1453 M Sh	I			
$\nu_{13}+\nu_{17}$ (1438, E_{1u})	$\nu_{13}+\nu_{17}$	1436 M	1435.9	7.5	1832.8	
	$\nu_{11}+\nu_{13}$	1399 W	I			
		1380 W Sh	I			
$\nu_{11}+\nu_{13}$ (1365, A_{2u}), $\nu_{10}+\nu_{16}$ (1365, E_{1u})	$\nu_{10}+\nu_{16}$	1364 M Sh	1365.0	7.0	2879.4	
$\nu_6+\nu_7$(1353, A_{2u})	$\nu_6+\nu_7$	1357 M	1356.9	7.7	7579.1	
$\nu_{15}-\nu_{14}$ (1340, E_{1u})		1343 M Sh	1343.5	7.1	1010.6	
		1339 M Sh	1338.7	7.7	590.4	
$\nu_{16}+\nu_{20}$ (1333, A_{2u})		1330 W Sh	1329.3	8.9	493.7	
		1319 W Sh	1319.8	4.7	91.7	
$\nu_7+\nu_{19}$ (1311, E_{1u})	$\nu_7+\nu_{19}$	1300 W	1303.0	9.2	522.5	
			1297.4	9.3	479.9	
$\nu_1-\nu_4$ (1275, A_{2u})	$\nu_{13}+\nu_{18}$	1272 W	1272.6	9.5	186.8	
$\nu_{13}+\nu_{18}$ (1259, E_{1u})	$\nu_{13}+\nu_{18}$	1262 W	1261.6	10.5	290.6	
		1247 W Sh	I			
		1219 W	1220.0	3.3	64.0	
$\nu_1-\nu_{14}$ (1175, E_{1u})		1179 W	I			
$\nu_{12}-\nu_{11}$ (1161, A_{2u})	$\nu_{12}-\nu_{11}$	1158 W	1157.9	11.1	1265.8	
		1136 W	I			
		1096 W Sh	I			
$\nu_{12}-\nu\nu_{17}$ (1088, E_{1u}) $\nu_6+\nu_{17}$ (1084, E_{1u})	$\nu_6+\nu_{17}$	1084 M	1084.7	6.2	957.0	
$\nu_5-\nu_8$ (1077, A_{2u})		1072 W	I			
$\nu_{17}+\nu_{19}$ (1042, A_{2u})	$\nu_{17}+\nu_{19}$	1045 M	1045.0	4.4	2775.1	
			1032.4	4.5	3709.0	
			1030.0	3.8	6865.3	
			1028.1	3.2	7781.4	
			1026.4	3.3	10651.7	
			1024.8	3.3	13006.2	
			1023.1	3.4	15085.0	
			1021.4	3.5	16721.9	
	$\nu_3+\nu_{14}$	1020 S	1019.7	3.6	17279.1	
			1017.9	3.7	17074.6	
$\nu_{15}-\nu_6$ (1014, E_{1u})		1015 S Sh	1016.0	4.1	18157.6	
			1013.9	4.5	19255.9	
			1011.5	4.9	19266.4	
$\nu_3+\nu_{14}$ (1009, E_{1u})		1007 S Sh	1008.8	5.0	17476.4	
			1006.2	5.0	15711.1	274239.2[e]
			1003.4	5.1	15015.1	
			1000.5	4.8	14975.6	
			997.9	4.8	24979.7	
ν_{13} (E_{1u})	ν_{13}	995 S	995.6	4.8	31837.5	
			993.3	4.9	33356.3	
			991.0	4.3	13009.1	
$\nu_9-\nu\nu_{18}$ (988, E_{1u})		987 S Sh	988.4	4.8	8827.7	
			985.0	4.9	5162.0	
$\nu_{16}-\nu_{20}$ (981, A_{2u})		982 S Sh	981.8	4.5	4778.9	
			978.7	4.5	3496.3	
$\nu_{12}-\nu_2$ (972, E_{1u}), $\nu_{11}+\nu_{19}$ (969, E_{1u})	$\nu_{11}+\nu_{19}$	972 M Sh	975.1	4.9	2026.4	
$\nu_{16}-\nu_{10}$ (951, E_{1u})		943 W Sh				
$\nu_7+\nu_{20}$ (888, E_{1u}),$\nu_6+\nu_8$ (889, A_{2u})	$\nu_7+\nu_{20}$	885 W	884.4	3.5	115.6	
$\nu_2+\nu_{14}$ (874, E_{1u}), $\nu_5-\nu_{17}$ (879, E_{1u})	$\nu_2+\nu_{14}$	872 W	872.2	5.3	276.3	
$\nu_{18}+\nu_{19}$ (863, A_{2u})		860 W	I			

Table 1 (*continued*)

Assignment[a]		Obsd $\tilde{\nu}^b$	Fitted band			Sum of C_j^c
Present works	Ref. [36]		$\tilde{\nu}^d$	Γ_j^d	C_j^c	
$\nu_8+\nu_{19}$ (844, E_{1u}),$\nu_{16}-\nu_{14}$ (842, E_{1u})	$\nu_8+\nu_{19}$	841 W	841.3	6.6	284.5	
$\nu_{12}-\nu_3$ (837, E_{1u})						
$\nu_9-\nu_{19}$ (809, E_{1u})		796 VW	I			
$\nu_2+\nu_4$ (774, A_{2u})	$\nu_2+\nu\nu_4$	779 VW	778.7	2.3	3.7	
$\nu_{14}+\nu_{17}$ (756, E_{1u})	$\nu_{14}+\nu_{17}$	757 W	I			
		741 VW Sh	I			
$\nu_{13}-\nu_{18}$ (731, E_{1u})		720 W Sh	723.2	8.6	76.5	
	$\nu_{13}-\nu_{18}$	718 W	718.7	5.0	60.4	
			716.1	18.6	0.0	
ν_7 (712, B_{2g})		711 VW Sh	I			
		662 VW Sh	664.0	18.4	49.0	
$\nu_{10}+\nu_{17}$ (649, E_{1u})	$\nu_{10}+\nu_{17}$	643 VW	647.8	12.4	54.5	
ν_6 (641, B_{1u})		641 VW Sh	639.1	11.0	55.8	
$\nu_{13}-\nu_{11}$ (625, A_{2u})		625 VW Sh	627.2	11.5	28.7	
$\nu_{17}+\nu_{20}$ (619, A_{2u})		615 VW	615.1	10.8	20.9	
ν_{19} (599, E_{2u})		603 VW	603.0	11.2	47.3	
		587 W Sh	591.0	10.7	45.0	
$\nu_4+\nu_{11}$ (585, E_{1u})	$\nu_4+\nu_{11}$	582 W	583.3	10.1	61.2	
$\nu_{14}+\nu_{18}$ (579, E_{1u})	$\nu\nu_{14}+\nu_{18}$	572 W	572.2	11.7	128.0	
$\nu_{16}-\nu_{19}$ (558, A_{2u})			561.8	26.4	8.0	
$\nu_{13}-\nu_{17}$ (552, E_{1u})	$\nu_{11}+\nu_{20}$	555 W	556.8	10.8	164.6	
$\nu_{11}+\nu_{20}$ (546, E_{1u})		551 W Sh	548.9	10.4	123.7	
$\nu_7-\nu_{20}$ (536, E_{1u})		529 W	529.3	8.2	65.2	
$\nu_{16}-\nu_6$ (516, E_{1u})	$\nu_{16}-\nu_6$	513 W Sh	515.8	10.9	40.7	
		510 W	508.7	11.1	48.2	
		506 W Sh				
$\nu_1-\nu_{13}$ (495, E_{1u})		496 VW Sh	497.4	12.2	32.5	
			485.9	13.3	23.2	
$\nu_{10}+\nu_{18}$ (470, E_{1u})	$\nu_{10}+\nu_{18}$	467 W Sh	471.8	12.9	50.8	
			464.7	10.2	30.8	
		455 W Sh	456.0	12.6	35.2	
$\nu_{18}+\nu_{20}$ (440, A_{2u})	$\nu_{18}+\nu_{20}$	442 W	441.2	22.6	311.1	
		408 W	407.8	12.6	100.5	
$\nu_3-\nu_{14}$ (379, E_{1u})		378 W Sh	378.7	6.6	16.9	
$\nu_6-\nu_{18}$ (377, E_{1u})		374 W Sh	373.5	5.6	20.5	
$\nu\nu_{11}$ (370, E_{1g})		370 W Sh	369.5	5.8	37.6	
		365 W	365.5	6.3	66.4	
		361 W Sh	360.2	6.7	40.3	
		354 W Sh	354.0	6.1	19.3	
$\nu_{19}-\nu_8$ (354, E_{1u})		347 W Sh	346.8	3.4	33.5	
$\nu_2-\nu_4$ (344, A_{2u})		343 W Sh	343.9	3.4	46.3	
		341 W Sh	341.2	3.1	37.5	
		338 W Sh	339.1	2.9	52.3	
		336 W Sh	337.0	2.8	50.7	
		334 W Sh	334.8	3.0	62.7	
			332.8	3.5	64.7	
$\nu_{19}-\nu_{18}$ (335, A_{2u})		329 W	329.3	4.3	99.0	
		324 M Sh	324.7	3.0	97.7	
			315.7	2.6	681.4	
ν_{14} (E_{1u})	ν_{14}	314 S	314.6	1.8	579.3	2798.9
			313.4	2.9	1385.7	
		309 M Sh	309.1	1.9	54.8	
$\nu_{13}-\nu_3$ (301, E_{1u})		304 W Sh	302.0	11.0	270.9	
		300 W Sh	I			
		298 W Sh	I			
		295 W Sh	I			
		290 W Sh	289.7	13.1	117.3	
		282 W Sh	I			
		279 W	280.5	9.1	131.9	
		276 W	276.7	3.1	25.0	
		273 W Sh	273.7	3.0	20.9	
$\nu_{17}-\nu_{20}$ (267, A_{2u})		269 W	270.3	5.0	106.1	
		267 W Sh	267.3	4.0	43.7	

Table 1 (*continued*)

Assignment[a]		Obsd $\tilde{\nu}$[b]	Fitted band			Sum of C_j[c]
Present works	Ref. [36]		$\tilde{\nu}$[d]	Γ_j[d]	C_j[c]	
$\nu\nu_{18}$ (264, E_{2g})		265 W Sh	264.9	4.5	46.0	
		260 W Sh	260.4	5.7	59.6	
		255 W Sh	254.7	7.4	94.5	

[a] Herzberg's notation is used to label the vibrations. The assignments are limited to fundamentals, first overtones and active binary combinations (sum and difference).
[b] The unit is cm^{-1}. VS, very strong; S, strong; M, medium; W, weak; VW, very weak; Sh, shoulder.
[c] The unit is cm mol^{-1}. Divide by 1×10^5 to convert to the usual unit of km mol^{-1}.
[d] The unit is cm^{-1}. I indicates the feature was ignored in the fit.
[e] Excludes intensity assigned to combinations.

the π-cloud of the nearest neighbour. The dipole moment derivatives of the gas were also recently [22] calculated via ab initio calculations using various levels of theory and basis sets.

This paper reports the fitting of the imaginary polarizability spectrum, α''_m, calculated under the Lorentz local field of hexafluorobenzene reported previously [16] between 4000 and 250 cm^{-1}. Most of the required peaks were due to observable features within the spectrum. The assignments of most of the features in the infrared spectrum of liquid hexafluorobenzene are reported.

In addition, ab initio calculations are used to facilitate the conversion of the derivatives from normal coordinates to internal coordinates. These derivatives are compared to the corresponding derivatives of benzene as well as the ab initio gas phase derivatives of hexafluorobenzene.

2. Experimental

2.1. Fitting the imaginary molar polarizability spectrum

By using the curvefitting program SPECFIT [23], the imaginary molar polarizability spectrum from 4000 to 254 cm^{-1} was fitted using classical damped harmonic oscillator bands. The fitting process began by splitting the full spectrum into three regions and fitting each separately. This allowed for changes in the fitted spectrum to be adjusted more quickly. The full spectrum was then fitted, refining the peaks from the separate regions. This fit required 274 peaks. The standard deviation of the fit is 0.011 $cm^3\ mol^{-1}$, the root-mean-square-error is 0.010 $cm^3\ mol^{-1}$, and the multiple coefficient of determination [24], R^2, is 0.99995, indicating a very good fit. The total area under the fitted spectrum between 4000 and 254 cm^{-1} is 0.69% larger than the corresponding area under the experimental spectrum.

SPECFIT outputs the peak wavenumber, $\tilde{\nu}_j$; the full width at half height (FWHH), Γ_j; and a constant, Y_j, that is the peak height of the corresponding band in the $\tilde{\nu}\alpha''_m$ spectrum multiplied by the FWHH. The complete integrated intensity under the α''_m band, C_j, can be obtained from Y_j through $C_j = Y_j\pi/2$. The parameters $\tilde{\nu}_j$, Γ_j, and C_j of the fitted bands are given in Table 1, as well as the observed positions of the features of the experimental spectrum. Several of the observed features were ignored in the fit. These were features next to much stronger ones where the uncertainties in fitting the stronger features were larger than the weaker features making any attempt to fit them meaningless.

The quality of the fit is shown in Fig. 1. On the true scale the spectra are superimposed, while small differences are visible on the expanded scale. In the top box of Fig. 1, visible differences occur at ~3930, ~3265, ~3214 and ~2800 cm^{-1}. In the middle box, visible differences occur at ~2700, ~2375, ~2200, ~2110, ~2050, ~1950, ~1850 and ~1650 cm^{-1}. In the bottom box, visible differences occur at ~1400, ~1150, ~950, and ~400 cm^{-1}. The majority of these differences (excluding those at ~1460, ~1440, ~1160, and ~400 cm^{-1}) are due to the broad wings of high absorbance bands in the region. The visible difference at ~400 cm^{-1} may be due to the usage of digitized data in this region [16].

In Fig. 2, the experimental and fitted spectra between 2550 and 2450 cm^{-1} are shown in the top box and the peaks used to calculate the fitted spectrum are shown in the bottom box. The wings of all spectra outside the region are included in the fitted spectrum but for clarity are not shown.

2.2. Ab initio calculations

All ab initio calculations presented in this paper were performed with Gaussian 03 Rev B.05 [25] on a dual processor 2.8 GHz Intel Xeon with 2 GB of RAM running under Red Hat Linux 8.0. The harmonic frequencies, harmonic force constants and dipole moment derivatives with respect to normal and internal coordinates of the isolated molecule were calculated at the CCD [26,27] level of theory with the cc-pVDZ [28–33] basis sets.

3. Results and discussion

Hexafluorobenzene belongs to the D_{6h} point group in the gas phase. It is expected that this will be a very good approximation for the liquid phase. The vibrational representation is $2A_{1g}+A_{2g}+A_{2u}+2B_{1u}+2B_{2g}+2B_{2u}+E_{1g}+3E_{1u}+4E_{2g}+2E_{2u}$. The A_{2u} and E_{1u} vibrations are infrared active in the gas phase while the A_{1g}, E_{1g}, and E_{2g} are Raman active in the gas phase. The A_{2g}, B_{1u}, B_{2g}, and E_{2u} are inactive in both the infrared and

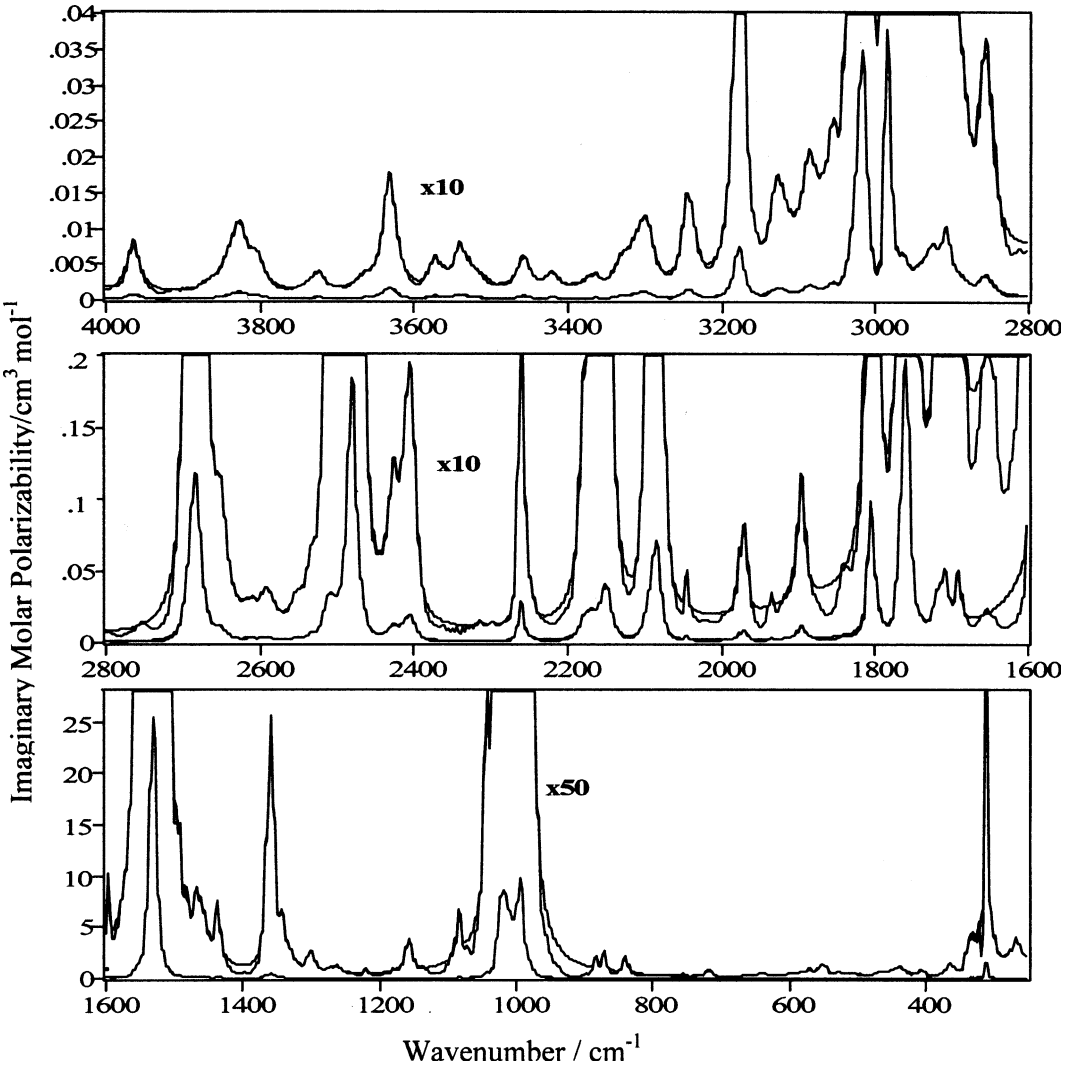

Fig. 1. The experimental and fitted imaginary molar polarizability spectra of liquid C_6F_6 at 25 °C between 4000 and 250 cm^{-1}. The upper spectra in top and middle boxes are the experimental and fitted spectra multiplied by 10. The upper spectra in the bottom box are the experimental and fitted spectra multiplied by 50.

Raman in the gas phase. This should also hold for the liquid although some of the inactive vibrations may be activated in the liquid [20]. This means that of the twenty fundamentals, only four can be determined from the infrared spectrum, and seven determined from the Raman. The remaining nine fundamentals have to be determined from the infrared or Raman active combinations. The $A_{1g}\times A_{2u}$, $A_{1g}\times E_{1u}$, $A_{2g}\times E_{1u}$, $B_{2g}\times B_{1u}$, $B_{2g}\times E_{2u}$, $E_{1g}\times A_{2u}$, $E_{2g}\times B_{1u}$, $E_{2g}\times B_{2u}$, $E_{1g}\times E_{1u}$, $E_{1g}\times E_{2u}$, $E_{2g}\times E_{1u}$, and $E_{2g}\times E_{2u}$ binary combinations are infrared active. The first overtones are infrared inactive.

3.1. Vibrational assignments

3.1.1. IR and Raman active fundamentals

The infrared and Raman active fundamentals were reported in several studies and have been summarized by Sverdlov [34] and Varsanyi [35]. These values are reported in Table 2 along with the values assigned from the present work. The infrared active fundamentals observed in the present work are relatively easy to assign. However, the Raman active fundamentals while not active in gas phase may be weakly active in the liquid phase. ν_1 is assigned to 1490 cm^{-1} in the Raman. The shoulder at 1492 cm^{-1} in the infrared spectrum, which cannot be assigned to any of the active binary combinations, could very well be ν_1. Similarly, there are features at 1655, 370, and 265 cm^{-1} that can not be assigned to any of the active binary combinations. These could be ν_{15}, ν_{11}, and ν_{18}, respectively.

3.2. Infrared active binary sum and difference bands

Steele and Whiffen [36] reported assignments for many of the combination bands observed in the infrared spectrum. These assignments were used along with the fundamentals given in Table 2 to assign the bands in the infrared spectrum. The assignments are reported in Table 1 along with those of Steele and Whiffen. The agreement between the observed wavenumbers of the current work and that of Steele and

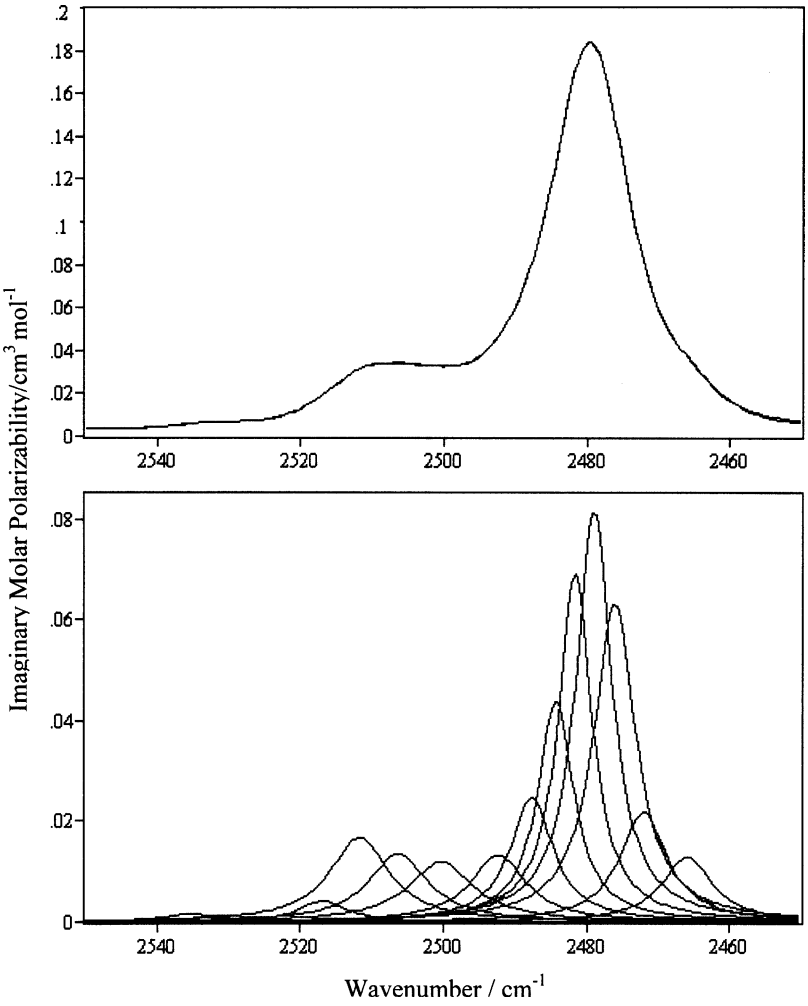

Fig. 2. The experimental and fitted imaginary molar polarizability spectra (top box) of liquid hexafluorobenzene at 25 °C between 2550 and 2450 cm^{-1} and the CDHO bands used to achieve the fit (bottom box). The wings of all peaks outside the region are included in the fitted spectrum but for clarity are not shown in the bottom box.

Whiffen is very impressive, especially considering that Steele and Whiffen were using a 1950 vintage spectrometer. We limited ourselves to the active binary combination bands because ternary bands would allow too many possibilities. However, from Table 1, it is obvious that many of the transitions cannot be assigned to infrared active binary combinations. These are either ternary or above transitions or inactive transitions that are activated in the liquid phase. A high quality spectrum of the gas to determine if these bands are present in the gas phase spectrum would be useful.

3.3. Inactive fundamentals

The inactive fundamentals are determined from active combinations. As stated above, the assignments of the present work and that of Steele and Whiffen are generally consistent, however, the present measurements allow the values of the inactive fundamentals to be refined. ν_3, ν_5, ν_6, ν_9, ν_{10}, ν_{19} and ν_{20} combine with fundamentals that are either Infrared or Raman active. Thus, the values of these fundamentals can be determined from the simple binary combinations. The ν_7 and ν_8 vibrations only combine with other inactive vibrations to generate active binary combinations. Therefore, these must be determined from combinations where both the fundamentals are inactive and the values of fundamentals ν_7 and ν_8 will be somewhat less certain than the others. The averages of the values determined in this way are reported in Table 2. Note that for ν_6, ν_7, ν_8 and ν_{20} the harmonic wavenumbers calculated at the CCD/cc-pVDZ level are lower than the anharmonic wavenumbers. This is opposite to the normal expectation and is probably due to inaccuracies in the ab initio values and/or a result of interactions of the combination bands used to determine these fundamentals with other active transitions.

3.4. Intensities of infrared active fundamentals

The integrated intensity, C_j, is related to the transition moment, R_j, under the assumption that the hot bands of the fundamental all contribute to the fundamental by

Table 2
Fundamental vibrations of hexafluorobenzene

Vibration	Symmetry	Activity	Anharmonic wavenumber/cm^{-1}			Harmonic wavenumber/cm^{-1}
			Present work[a]	Ref. [34]	Ref. [35]	Ab initio CCD/cc-pVDZ
ν_1	A_{1g}	Raman		1490	1490	1572
ν_2	A_{1g}	Raman		559	559	573
ν_3	A_{2g}	Inactive	694	691	691	789
ν_4	A_{2u}	Infrared		215	215	230
ν_5	B_{1u}	Inactive	1322	1323	1323	1379
ν_6	B_{1u}	Inactive	641	640	640	599
ν_7	B_{2g}	Inactive	712	714	714	654
ν_8	B_{2g}	Inactive	245	249	249	188
ν_9	B_{2u}	Inactive	1252	1253	1253	1288
ν_{10}	B_{2u}	Inactive	206	208	208	273
ν_{11}	E_{1g}	Raman		370	370	410
ν_{12}	E_{1u}	Infrared	1530.7	1531	1530	1613
ν_{13}	E_{1u}	Infrared	995.6	1002	1011	1035
ν_{14}	E_{1u}	Infrared	314.6	315	315	318
ν_{15}	E_{2g}	Raman		1655	1655	1746
ν_{16}	E_{2g}	Raman		1157	1157	1206
ν_{17}	E_{2g}	Raman		443	443	448
ν_{18}	E_{2g}	Raman		264	264	266
ν_{19}	E_{2u}	Inactive	599	595	595	667
ν_{20}	E_{2u}	Inactive	176	175	175	139

[a] Values of the inactive fundamentals were determined from active binary combinations, see text for details.

[3,37–39]

$$C_j = \frac{N_A \pi}{3hc_0} g_j \nu_j |\boldsymbol{R}_j|^2 \quad (1)$$

where N_A is Avogadro's number, h is Planck's constant, c_0 is the speed of light in a vacuum, g_j is the degeneracy of the transition, and is the vibrational wavenumber. The integrated intensity can also be related to the square of the dipole moment derivative with respect to the jth normal coordinate, $\mu_j^2 = |\partial\vec{\mu}/\partial Q_j|^2$, under the double harmonic approximation by [3]

$$C_j = \frac{N_A}{24\pi c_0^2} g_j \mu_j^2 \quad (2)$$

The transition moments and square of the dipole moment derivatives of the fundamentals of hexafluorobenzene are given in Table 3 along with those previously reported [7,8] for benzene-h_6 and benzene-d_6.

Under the double harmonic approximation, the integrated intensities of different isotopomers can be compared by the F-Sum rule [40,41]. In addition to the requirements of the double harmonic approximation, the F-sum is only applicable if either the molecule does not have a permanent dipole moment or if the summation is over vibrations that belong to a symmetry species that does not involve a rotation of the permanent dipole of the molecule. The F-sum, expressed in terms of C_j and $\tilde{\nu}_j$, is

$$\sum \frac{C_j}{\nu_j^2} = \text{constant} \quad (3)$$

For the intensities given in Table 1, Eq. (3) equates to 0.559 cm^3 mol^{-1} for hexafluorobenzene as compared to 0.030 cm^3 mol^{-1} for benzene-h_6 [7] and 0.031 cm^3 mol^{-1} for benzene-d_6 [8]. This confirms that the differences in intensities are not merely due to differences in the normal coordinates but rather, as is expected, due to significant differences in the dipole moment derivatives with respect to internal coordinates.

To convert from dipole moment derivatives with respect to normal coordinates to derivatives with respect to symmetry or internal coordinates requires a force field analysis. With only data for one isotopomer, it is impossible to do a complete force field analysis based on the experimental data. Even for the E_{1u} vibrations this would require six force constants and there is

Table 3
Transition moments and dipole moment derivatives with respect to normal coordinates for hexafluorobenzene, benzene-h_6 and benzene-d_6

Vibration	C_6F_6(ℓ)		C_6F_6(g)		C_6H_6(ℓ) [7]		C_6D_6(ℓ) [8]	
	$\lvert R_j\rvert/D$	$\lvert\mu\rvert$/(D Å^{-1} u$^{-1/2}$)	$\lvert R_j\rvert/D$	$\lvert\mu_j\rvert$/(D Å^{-1} u$^{-1/2}$)	$\lvert R_j\rvert/D$	$\lvert\mu_j\rvert$/(D Å^{-1} u$^{-1/2}$)	$\lvert R_j\rvert/D$	$\lvert\mu_j\rvert$/(D Å^{-1} u$^{-1/2}$)
ν_4	Not measured		0.105	0.38	0.242	1.53	0.199	1.09
ν_{12}	0.247	2.36	0.283	2.76	0.0533	0.715	0.0434	0.505
ν_{13}	0.208	1.60	0.307	2.40	0.0515	0.482	0.0284	0.252
ν_{14}	0.0374	0.162	0.0467	0.203	0.0458	0.359	0.0528	0.367

only sufficient data to determine three. It was found earlier [21], that there is no significant difference between the liquid and gas force fields of benzene. It was also shown [22] that ab initio calculations can be used to successfully obtain information about the force field and dipole moment derivatives of the gas. As such, the force field and dipole moment derivatives of hexafluorobenzene were determined at the CCD [26,27] level of theory with the cc-pVDZ [28–33] basis set, as was done for benzene [22]. This level of theory should give results for the gas-phase accurate enough to draw conclusions about the differences between the gas and the liquid intensities.

The calculated harmonic wavenumbers of the gas are included in Table 2 and the harmonic force constants are given in Table 4. It is interesting to compare the force constants to those calculated for benzene at the same level of theory and with the same basis set. As expected, the largest difference in the force constants is for the terms that involve the fluorine or hydrogen atoms. However, the differences between the force constants involving only the carbons of hexafluorobenzene and benzene are much smaller with at most a 5% difference in the diagonal elements. The off-diagonal elements involving only the carbons vary by less than 0.06 mdyne $Å^{-1}$. Somewhat surprisingly, the out-of-plane force constants involving the fluorine or hydrogen atoms differ less than those for the carbons. The out-of-plane diagonal force constant for the FCCC torsion (f_{27}) differs from the HCCC torsion force constant in benzene by only 0.165 mdyne $Å^{-1}$ while the out-of-plane carbon torsion CCCC force constants and the off-diagonal elements differ by less than 0.08 mdyne $Å^{-1}$. Clearly, the distortions of the phenyl ring are very similar in the two molecules despite the drastically different charge distributions.

Table 4
Internal coordinate force constants of hexafluorobenzene and benzene at CCD level of theory with cc-pVDZ basis set

Force constant	Potential term	Hexafluoroben-zene	Benzene [22]
f_1	t_it_i	7.456	7.120
f_2	s_is_i	7.299	5.666
f_3	$R_{19}R_{19}$	1.326	1.283
f_4	$R_{20}R_{20}$	1.337	1.286
f_5	$R_{13}R_{13}$	0.881	0.539
f_6	t_it_{i+1}	0.768	0.770
f_7	t_it_{i+2}	−0.555	−0.530
f_8	t_it_{i+3}	0.415	0.477
f_9	s_is_{i+1}	0.133	0.010
f_{10}	s_is_{i+2}	0.054	0.003
f_{11}	s_is_{i+3}	0.100	0.001
f_{12}	$R_{13}R_{14}$	0.034	0.009
f_{13}	$R_{13}R_{15}$	−0.034	−0.013
f_{14}	$R_{13}R_{16}$	−0.003	−0.002
f_{15}	t_is_i	0.366	0.068
f_{16}	t_is_{i+2}	0.016	−0.005
f_{17}	t_is_{i+3}	−0.086	−0.018
f_{18}	t_1R_{20}	0.079	0.127
f_{19}	s_1R_{19}	−0.300	−0.113
f_{20}	s_1R_{20}	−0.403	−0.105
f_{21}	t_1R_{13}	0.236	0.160
f_{22}	t_1R_{15}	0.063	−0.015
f_{23}	t_1R_{16}	−0.016	0.023
f_{24}	s_1R_{14}	0.094	0.008
f_{25}	s_1R_{15}	−0.015	−0.008
f_{26}	$R_{14}R_{20}$	−0.114	−0.076
f_{27}	$\gamma_i\gamma_i$	0.640	0.475
f_{28}	$R_{28}R_{28}$	0.383	0.402
f_{29}	$R_{29}R_{29}$	0.411	0.338
f_{30}	$\gamma_i\gamma_{i+1}$	−0.136	−0.071
f_{31}	$\gamma_i\gamma_{i+2}$	0.011	0.002
f_{32}	$\gamma_i\gamma_{i+3}$	0.019	−0.022
f_{33}	γ_1R_{28}	0.210	0.170
f_{34}	γ_1R_{29}	−0.242	−0.163

The unit of the force constants is mdyne $Å^{-1}$.

The transition moments and dipole moment derivatives with respect to the normal coordinates of the gas calculated at the CCD/cc-pVDZ level are included in Table 3. It is clear that there are significant differences between transition moments and dipole moment derivatives with respect to normal coordinates in the liquid and gas states. The next logical question is "how do these differences compare to the differences determined for benzene?" [21,42].

In order to compare the intensities between the liquid and gas as well as to those of benzene it is necessary to convert the dipole moment derivatives to internal coordinates. The same definitions of the internal coordinates are used in the present work as were used in the benzene work [20]. The Gaussian checkpoint file includes the dipole moment derivatives with respect to the Cartesian coordinates. It is a simple transformation to convert these dipole moment derivatives to internal coordinates. These are given in Table 5.

The conversion of the liquid dipole moment derivatives with respect to normal coordinates to internal coordinates is a little more complicated. The dipole moment derivatives with respect to internal coordinates are linear combinations of the dipole moment derivatives with respect to normal coordinates. The coefficients of the transformation are obtained from the eigenvectors of the force field. However, since only the magnitude of the dipole moment derivatives with respect to normal coordinates can be obtained from the experimental intensities, it is necessary to consider the different sign combination of the dipole moment derivatives with respect to normal coordinates. With three dipole moment derivatives with respect to normal coordinates, there are eight possible combinations. They are $+++$, $++-$, $+-+$, $+--$, $---$, $--+$, $-+-$, and $-++$. The second four give the same magnitude of the dipole moment derivatives with respect to internal coordinates as the first four, respectively, but the dipole moment derivatives are anti-parallel. Included in Table 5, are the dipole moment derivatives for the second set of four sign combinations. The dipole moment derivatives with respect to the internal coordinates vary significantly for the different sign combination. While it is expected that the intermolecular interactions in the liquid will alter the dipole moment derivatives, it is not expected that this will be so drastic as to change the direction of the dipole moment derivatives, especially given the magnitude of the dipole moment derivatives considered here. The $--+$ combination gives the same direction for the dipole moment derivatives with respect to internal coordinates of the liquid as those of the gas as well as the best agreement between the derivatives in the

Table 5
Dipole moment derivatives with respect to internal coordinates for hexafluorobenzene and benzene

Molecule	$\partial\mu_y/\partial s_1$	$\partial\mu_x/\partial t_2$	$\partial\mu_x/\partial\beta_1$	$\partial\mu_z/\partial\gamma_1$
C_6F_6(g)	−5.53	1.03	0.78	−0.57
C_6F_6(ℓ)− − −	−4.37	0.06	−0.13	
C_6F_6(ℓ)− − +	−4.00	1.27	0.50	
C_6F_6(ℓ)− + −	0.79	3.16	−1.15	
C_6F_6(ℓ)− + +	1.16	4.38	−0.52	
$C_6H_6/C_6D_6/C_6H_5D$(ℓ) [20,22]	−0.38(2)	−0.24(1)	−0.26(1)	0.64(3)
C_6H_6/C_6D_6(g) [21,22]	−0.50(3)	−0.28(3)	−0.24(1)	0.65(2)

two phases. This combination is taken as the correct combination.

From the results in Table 5, one can see that the magnitude of the dipole moment derivative for the CF stretching coordinate is smaller in the liquid. This is consistent with what was observed for benzene [21,42]. For benzene it was postulated [21] that this difference is due to the interaction of the hydrogen with the π-cloud of the neighbouring benzene molecule. However, the magnitude of the dipole moment derivatives for the CC stretch and FCC bend also vary significantly between the liquid and gas, whereas for benzene the corresponding derivatives are basically constants. This indicates that the in-plane motions are more sensitive to the intermolecular interactions in hexafluorobenzene that in benzene.

It would be interesting to see the effect on the out-of-plane dipole moment derivative, however, this fundamental lies outside the range of the spectrometer currently available to this laboratory. This laboratory has recently been successful in obtaining funding to purchase a new FTIR spectrometer capable of measuring in the far-IR. Once this spectrometer is in place, the measurement of the low wavenumber spectrum of hexafluorobenzene will be one of the first measurements carried out.

It is also worthwhile to compare the dipole moment derivatives with respect to internal coordinates of hexafluorobenzene to those of benzene for both the liquid and gas states. The magnitude of $\partial\mu_y/\partial s_1$ is approximately an order of magnitude larger for hexafluorobenzene than for benzene indicating that there is a much greater charge redistribution for the CF bond stretch than for the CH bond stretch. This is due to the much greater charge on the fluorine atoms than the hydrogen atoms and the resulting effect on the electron density in the π-cloud. $\partial\mu_y/\partial s_1$ has the same sign in both molecules, whereas the other dipole moment derivatives with respect to internal coordinates have opposite signs in the two molecules.

In the gas phase the magnitude of $\partial\mu_x/\partial t_2$ is approximately 4× larger for hexafluorobenzene than for benzene while in the liquid phase it is approximately 5× larger. This reflects the fact that there is a smaller electron density in the π-cloud of hexafluorobenzene and as such it is more susceptible to distortions of the ring. Spedding and Whiffen [43] defined the ring contribution to the CC stretching derivative as $(\partial\mu_x/\partial t_2)_{\text{ring}} = \partial\mu_x/\partial t_2 - R_{\text{CC}}^{-1}\sqrt{1.5}(\partial\mu_x/\partial\beta_1)$. Using the values of $\partial\mu_x/\partial t_2$ for the gas and liquid phases, gives $(\partial\mu_x/\partial t_2)_{\text{ring}} =$ 0.35 Debye Å^{-1} for the gas and 0.83 for the liquid, whereas it was found [22] that for both phases of benzenes $(\partial\mu_x/\partial t_2)_{\text{ring}} = -0.07$ Debye Å^{-1}. Again, this indicates that the electrons in the π-cloud of hexafluorobenzene are more polarizable due to the electron withdrawing nature of the F.

In the gas phase the magnitude of $\partial\mu_x/\partial\beta_1$ is approximately 3× larger for hexafluorobenzene than for benzene while in the liquid phase it is approximately 2× larger. These derivatives have opposite signs in hexafluorobenzene compared to benzene due to the opposite partial charges on the fluorines and hydrogens. The larger magnitude indicates that in hexafluorobenzene much more of the charge is localized on the terminal atoms and thus the π-cloud has a lower electron density in hexafluorobenzene.

In the gas phase the magnitude of $\partial\mu_z/\partial\gamma_1$ is approximately only 12% smaller for hexafluorobenzene than for benzene and points in the opposite direction. The opposite direction is due to the opposite charge on the fluorine and hydrogen atoms. Somewhat surprisingly, the magnitudes are very similar. This indicates that the out-of-plane motion to a large extent does not depend on the charge distribution. To test this further it would be worthwhile to explore this in other substituted benzenes.

As was done previously [22] for benzene, it is useful to think of the bending vibration dipole moment derivatives with respect to internal coordinates in terms of electrons instead of Debye Å^{-1}. 1 Debye equals 0.208e Å, and thus, the dipole moment derivatives in Table 5, give −0.119e for the out-of-plane F torsion and 0.162e for the in-plane FCC deformation in the gas and 0.104e for the in-plane FCC deformation in the liquid. Note that in the FCC motion, the F moves in the negative x direction for a positive deformation and thus, both of these imply a C^+F^- partial charge arrangement, during each of these motions. The partial charges for these motions are different as is the case for benzene [21,22], and is consistent with the work of Spedding and Whiffen [43] suggesting different contributions from the π-electron densities for the in-plane and out-of-plane bending distortions.

4. Summary

In this paper, the imaginary molar polarizability spectrum of liquid hexafluorobenzene was fitted to CDHO bands. Most of the required bands were obvious in the experimental spectrum and many were assigned to infrared active fundamentals or

binary combinations. From the active combination transitions, the wavenumbers of the inactive fundamentals were obtained. The integrated intensities of the infrared active fundamentals were determined from the parameters of the fitted bands and used to determine the transition moments and dipole moment derivatives with respect to normal coordinates for the liquid.

Ab initio calculations were performed to determine the harmonic force constants and the dipole moment derivatives with respect to the internal coordinates of the gas phase. These dipole moment derivatives were compared to the corresponding liquid phase derivatives as well as to the dipole moment derivatives of benzene. The differences between the liquid and gas phase dipole moment derivatives of hexafluorobenzene were found to be consistent with those previously reported for benzene.

References

[1] E.B. Wilson Jr., Phys. Rev. 45 (1934) 706.
[2] J.E. Bertie, S.L. Zhang, C.D. Keefe, Vib. Spectrosc. 8 (1995) 215.
[3] J.E. Bertie, S.L. Zhang, C.D. Keefe, J. Mol. Struct. 324 (1994) 157.
[4] C.D. Keefe, J. Mol. Spectrosc. 205 (2001) 261.
[5] J.E. Bertie, C.D. Keefe, R.N. Jones, Can. J. Chem. 69 (1991) 1609.
[6] J.E. Bertie, R.N. Jones, C.D. Keefe, Appl. Spectrosc. 47 (1993) 891.
[7] J.E. Bertie, C.D. Keefe, J. Mol. Struct. 695–696 (2004) 39.
[8] J.E. Bertie, C.D. Keefe, Fresenius J. Anal. Chem. 362 (1998) 91.
[9] J.E. Bertie, Y. Apelblat, C.D. Keefe, J. Mol. Struct. 550–551 (2000) 135.
[10] C.D. Keefe, J. Pittman, Appl. Spectrosc. 52 (1998) 1062.
[11] C.D. Keefe, L.A. Donovan, S.D. Fleet, J. Phys. Chem. A 103 (1999) 6420.
[12] C.D. Keefe, L.A. Donovan, J. Mol. Struct. 597 (2001) 259.
[13] C.D. Keefe, J.K. Pearson, J. Mol. Struct. 751 (2005) 190.
[14] J.E. Bertie, R.N. Jones, Y. Apelblat, C.D. Keefe, Appl. Spectrosc. 48 (1994) 127.
[15] J.E. Bertie, Y. Apelblat, C.D. Keefe, J. Mol. Struct. 750 (2005) 78.
[16] C.D. Keefe, S. MacInnis, T. Burchell, J. Mol. Struct. 610 (2002) 253.
[17] C.D. Keefe, E. Brand, J. Mol. Struct. 691 (2004) 181.
[18] C.D. Keefe, J. Barrett, L.L. Jessome, J. Mol. Struct. 734 (2005) 67.
[19] C.D. Keefe, J.K. Pearson, A. MacDonald, J. Mol. Struct. 655 (2003) 69.
[20] C.D. Keefe, J.E. Bertie, Spectrochimica. Acta Part A, Submitted for publication.
[21] C.D. Keefe, J.E. Bertie, Spectrochimica. Acta Part A, Submitted for publication.
[22] C.D. Keefe, Chem. Phys., Submitted for publication.
[23] C.D. Keefe, J. Mol. Struct. 641 (2002) 165.
[24] J. McClave, F. Dietrich, T. Sincich, in: Statistics, seventh ed., Prentice-Hall, Upper Saddle River, 1997, pp. 553–554.
[25] M.J. Frisch, G.W. Trucks, H.B. Schlegel, G.E. Scuseria, M.A. Robb, J.R. Cheeseman, J.A. Montgomery, Jr., T. Vreven, K.N. Kudin, J.C. Burant, J.M. Millam, S.S. Iyengar, J. Tomasi, V. Barone, B. Mennucci, M. Cossi, G. Scalmani, N. Rega, G.A. Petersson, H. Nakatsuji, M. Hada, M. Ehara, K. Toyota, R. Fukuda, J. Hasegawa, M. Ishida, T. Nakajima, Y. Honda, O. Kitao, H. Nakai, M. Klene, X. Li, J.E. Knox, H.P. Hratchian, J.B. Cross, C. Adamo, J. Jaramillo, R. Gomperts, R.E. Stratmann, O. Yazyev, A.J. Austin, R. Cammi, C. Pomelli, J.W. Ochterski, P.Y. Ayala, K. Morokuma, G.A. Voth, P. Salvador, J.J. Dannenberg, V.G. Zakrzewski, S. Dapprich, A.D. Daniels, M.C. Strain, O. Farkas, D.K. Malick, A.D. Rabuck, K. Raghavachari, J.B. Foresman, J.V. Ortiz, Q. Cui, A.G. Baboul, S. Clifford, J. Cioslowski, B.B. Stefanov, G. Liu, A. Liashenko, P. Piskorz, I. Komaromi, R.L. Martin, D.J. Fox, T. Keith, M.A. Al-Laham, C.Y. Peng, A. Nanayakkara, M. Challacombe, P.M.W. Gill, B. Johnson, W. Chen, M.W. Wong, C. Gonzalez, J.A. Pople, GAUSSIAN 03, Revision B.05, Gaussian, Inc., Pittsburgh PA, 2003.
[26] J.A. Pople, R. Krishnan, H.B. Schlegel, J.S. Binkley, Int. J. Quantum. Chem. Symp. XIV (1978) 545.
[27] R.J. Bartlett, G.D. Purvis, Int. J. Quantum. Chem. Symp. 14 (1978) 516.
[28] R.A. Kendall, T.H. Dunning Jr., R.J. Harrison, J. Chem. Phys. 96 (1992) 6796.
[29] T.H. Dunning Jr., J. Chem. Phys. 90 (1989) 1007.
[30] D.E. Woon, T.H. Dunning Jr., J. Chem. Phys. 98 (1993) 1358.
[31] K.A. Peterson, D.E. Woon, T.H. Dunning Jr., J. Chem. Phys. 100 (1994) 7410.
[32] E.R. Davidson, Chem. Phys. Lett. 220 (1996) 514.
[33] A. Wilson, T. van Mourik, T.H. Dunning Jr., J. Mol. Struct. (Theochem) 388 (1997) 339.
[34] L.M. Sverdlov, M.A. Kovner, E.P. Krainov, Vibrational Spectra of Polyatomic Molecules, Halsted Press, New York, 1974.
[35] G. Varsanyi, Assignments for Vibrational Spectra of Seven Hundred Benzene Derivatives, vol. 1, Wiley, New York, 1974.
[36] D. Steele, D.H. Whiffen, Trans. Faraday Soc. 55 (1959) 369.
[37] J. Fahrenfort, in: M. Davies (Ed.), Infra-Red Spectroscopy and Molecular Structure: an Outline of the Principles, Elsevier, Amsterdam, 1963.
[38] J.W. Warner, M. Wolfsberg, J. Chem. Phys. 78 (1983) 1722.
[39] M.J. Dignam, Appl. Spectrosc. Rev. 21 (1988) 99.
[40] B. Crawford Jr., J. Chem. Phys. 20 (1952) 977.
[41] J.C. Decius, J. Chem. Phys. 20 (1952) 1039.
[42] J.E. Bertie, C.D. Keefe, J. Chem. Phys. 101 (1994) 4610.
[43] H. Spedding, D.H. Whiffen, Proc. R. Soc. 238A (1956) 245.